Minimal Model of Solitons in Nematic Liquid Crystals

Noe Atzin,[1,*] Ali Mozaffari,[1,2,*] Xingzhou Tang,[1,*] Soumik Das,[3,4] Nicholas L. Abbott,[4] and Juan J. de Pablo[1,5,†]
[1]Pritzker School of Molecular Engineering, The University of Chicago, Chicago, Illinois 60637, USA
[2]OpenEye, Cadence Molecular Sciences, Boston, Massachusetts 02114, USA
[3]Department of Chemical Engineering, Indian Institute of Technology Kanpur, Kanpur, 208016, India
[4]Smith School of Chemical and Biomolecular Engineering, Cornell University, Ithaca, New York 14853, USA
[5]Center for Molecular Engineering, Argonne National Laboratory, Lemont, Illinois 60439, USA

(Received 20 October 2022; revised 20 June 2023; accepted 11 September 2023; published 30 October 2023)

Solitons in liquid crystals have generated considerable interest. Several hypotheses of varying complexity have been advanced to explain how they arise, but consensus has not emerged yet about the underlying forces responsible for their formation or their structure. In this work, we present a minimal model for solitons in achiral nematic liquid crystals, which reveals the key requirements needed to generate them in the absence of added charges. These include a surface inhomogeneity, consisting of an adsorbed particle capable of producing a twist, flexoelectricity, dielectric contrast, and an applied ac electric field that can couple to the director's orientation. Our proposed model is based on a tensorial representation of a confined liquid crystal, and it predicts the formation of "butterfly" structures, quadrupolar in character, in regions of a slit channel where the director is twisted by the surface imperfection. As the applied electric field is increased, solitons (or "bullets") become detached from the wings of the butterfly, and then propagate rapidly throughout the system. The main observations that emerge from the model, including the formation and structure of butterflies, bullets, and stripes, as well as the role of surface inhomogeneity and the strength of the applied field, are consistent with experimental findings presented here for nematic LCs confined between two chemically treated parallel plates.

DOI: 10.1103/PhysRevLett.131.188101

Traveling waves that propagate without distorting their shape or losing energy are referred to as solitons; they have been studied extensively in isotropic liquids [1,2]. Solitons were first described by Russell *et al.* over 150 years ago (1834), who studied how waves in water propagate at constant speed in a narrow channel [3]. The structures associated with solitons in liquid crystals (LCs) were first discussed by de Gennes and Leger [4,5], and their quadrupolar structure (butterfly) was originally reported in experiments by Brand *et al.* [6]. In achiral nematic liquid crystals, recent work indicates that solitons can be produced by applying an electric field [7–13]. After a collision, solitons preserve their shape, thereby providing opportunities for the design of autonomous materials that rely on energy transduction for active transport [14–18].

Recent experimental work by our group has revealed that surface interactions play a decisive and previously unappreciated role in the generation and dynamics of solitons [19,20]. However, the precise structure of a nematic soliton or the forces that lead to its creation remain unknown. Simulations of the formation and structure of solitons have not been reported before. In this work, we propose a minimal model that reproduces the central features of solitons observed in experiments. With that model, we show that surface imperfections serve to nucleate solitons, we find that their structure is a function of the applied electric field, and we dissect how the balance of free energy contributions from flexoelectricity, surface anchoring, and elasticity is altered throughout the soliton formation process. We also present the results of controlled experiments that serve to validate the predictions of our model.

Methodology.—Theoretical framework: The free energy functional of the tensorial order parameter ($\mathbf{Q}$) is written in the form of $\mathbf{Q} = S(\mathbf{nn} - \mathbf{I}/3)$, where the unit vector $\mathbf{n}$ is the director field and S is the scalar order parameter [21]. We introduce an alternating current field (ac) that couples to the director via a negative anisotropy of the permittivity of the liquid crystal. The liquid crystal is confined between two walls, and a surface irregularity is created by appending a hemispherical particle to one of the walls. $\mathbf{Q}$ is evolved through the Ginzburg-Landau equation [22–25]:

$$\frac{\partial}{\partial t}\mathbf{Q} = \Gamma\mathbf{H};\ \ \mathbf{H} = -\left(\frac{\delta\mathcal{F}}{\delta\mathbf{Q}} - \frac{\mathbf{I}}{3}\mathrm{Tr}\frac{\delta\mathcal{F}}{\delta\mathbf{Q}}\right). \tag{1}$$

where Γ is a collective rotational diffusion constant that controls the relaxation rate, and $\mathbf{H}$ is the molecular field.

The free energy of the system is given by

$$\mathcal{F} = \int_V [f_{\mathrm{LdG}} + f_{\mathrm{elas}} + f_{\mathrm{flex}} + f_{\mathrm{diel}}]dV + \int_S [f_{\mathrm{H}} + f_{\mathrm{P}}]dS, \tag{2}$$

and the bulk free energy density is given by the sum of an enthalpic contribution (f_{LdG}), an elasticity contribution (f_{elas}), a flexoelectricity contribution (f_{flex}), and a dielectric energy contribution (f_{diel}). At the confining boundaries, dS has unit normal $\boldsymbol{\nu}$. Anchoring conditions can be imposed by adding a surface term to the free energy [26,27].

The enthalpic term is given by [28]

$$f_{\mathrm{LdG}} = \frac{A}{2}\left(1-\frac{U}{3}\right)\mathrm{Tr}(\mathbf{Q})^2 - \frac{AU}{3}\mathrm{Tr}(\mathbf{Q}^3) + \frac{AU}{4}(\mathrm{Tr}(\mathbf{Q^2}))^2, \tag{3}$$

where A and U are phenomenological parameters [29,30]. In the second term, the elastic distortions can be written as [31,32]

$$f_{\mathrm{elas}} = \frac{1}{2}L_1\partial_k Q_{ij}\partial_k Q_{ij} + \frac{1}{2}L_2\partial_k Q_{jk}\partial_l Q_{jl} + \frac{1}{2}L_3 Q_{ij}\partial_i Q_{kl}\partial_j Q_{kl}. \tag{4}$$

In this work, we include L_1 and L_3 and assume $L_2 = 0$. In the presence of an externally applied electric field, a flexoelectric contribution to the free energy arises from the coupling between the nematic distortion and polarization [33–35]:

$$f_{\mathrm{flex}} = E_i P_i = \zeta_1(\partial_j Q_{ij})E_i + \zeta_2 Q_{ij}(\partial_k Q_{jk})E_i. \tag{5}$$

The dielectric energy contribution is given by [36,37]

$$f_{\mathrm{diel}} = -\frac{1}{2}\epsilon_0\epsilon_{ij}E_iE_j, \tag{6}$$

where ϵ_0 represents the dielectric permittivity of vacuum, and ϵ_{ij} corresponds to the tensorial dielectric permittivity of the nematic material [38,39]. The above expressions can be rewritten in terms of the $\mathbf{Q}$ tensor as

$$f_{\mathrm{diel}} = -\frac{1}{2}\epsilon_0\epsilon_a E_i Q_{ij} E_j, \tag{7}$$

and ϵ_a is the permittivity anisotropy.

A hybrid anchoring of the director field is enforced at the surface. Homeotropic anchoring at a particle surface (see below) is imposed using a Rapini-Papoular surface free energy density of the form [40,41]

$$f_{\mathrm{H}} = \frac{1}{2}W(\mathbf{Q}-\mathbf{Q^0}), \tag{8}$$

which penalizes deviations from the surface-preferred tensorial order parameter $\mathbf{Q}^0 = S_{\mathrm{eq}}(\boldsymbol{\nu\nu} - \mathbf{I}/3)$. A fourth-order Fournier-Galatola free energy density is adopted to impose degenerate planar anchoring at the walls [42]

$$f_P = \frac{1}{2}W(\bar{\mathbf{Q}}-\bar{\mathbf{Q}}_\perp)^2 + \frac{1}{4}W(\bar{\mathbf{Q}}:\bar{\mathbf{Q}} - S_{\mathrm{eq}}^2)^2, \tag{9}$$

where W controls the anchoring strength, $\bar{\mathbf{Q}} = \mathbf{Q} + (1/3)S_{\mathrm{eq}}\mathbf{I}$ and its projection on the surface is given by $\bar{\mathbf{Q}}_\perp = \mathbf{p}\cdot\bar{\mathbf{Q}}\cdot\mathbf{p}$, with $\mathbf{p} = \mathbf{I} - \boldsymbol{\nu\nu}$. An effective electric field (EF^*) can be defined using the ratio between the flexoelectric term and the elastic energy,

$$EF^* = \frac{\zeta_2}{L_1}E_i. \tag{10}$$

Additional details of the theoretical framework and numerical details are provided in the Supplemental Material [43], which includes Refs. [44–47].

Experimental system: Our experiments correspond to 4′-butyl-4-heptyl-bicyclohexyl-4-carbonitrile (CCN-47) confined between two surfaces pretreated with self-assembled monolayers (SAMs) of alkanethiols on obliquely deposited thin gold films. Prior studies have established that SAMs of $C_{16}SH$ cause planar anchoring of this material [19]. Additional details of the preparation of the surfaces are provided in the Supplemental Material [43]. Here we merely point out that we dispersed 3 μm polyethylene (PE) particles in CCN-47, and the mixture was drawn into the optical cell by capillary action at 70° ($T > T_{NI}$), followed by cooling to the nematic phase ($T = 45°\,\mathrm{C}$). Such particles serve as the site for the nucleation of solitons. The nematic phase of CCN-47 at 45° C adopts a uniform azimuthal orientation on the surfaces.

Results and discussion.—Consistent with our experimental system, our model corresponds to a nematic liquid crystal confined within walls that impart strong planar anchoring. In the absence of an imposed surface inhomogeneity, the director field remains in a homogeneous state. A small hemispherical particle with homeotropic anchoring is then placed at the center of the bottom wall; its radius is one-fifth of the channel thickness (Fig. 1). This particle introduces a small distortion into an otherwise homogeneous structure. An oscillatory electric field is applied normal to the confining boundaries (Z axis). To better represent the experimental conditions and to control the direction of motion of the solitons, a slight dc offset and white noise are superimposed on the ac electric field (see Fig. S1 in the Supplemental Material [43]). The director field is initially aligned along the X axis, with periodic boundary conditions in the X and Y directions [Fig. 1(b)]. Since the simulated system is two orders of magnitude smaller than our typical experimental device, the intensity of the electric field and the size of the director structures are different than those used in experiments. However, when properly normalized using the effective electric field (EF^*), one can see that the experimental and simulated structures exhibit comparable behaviors.

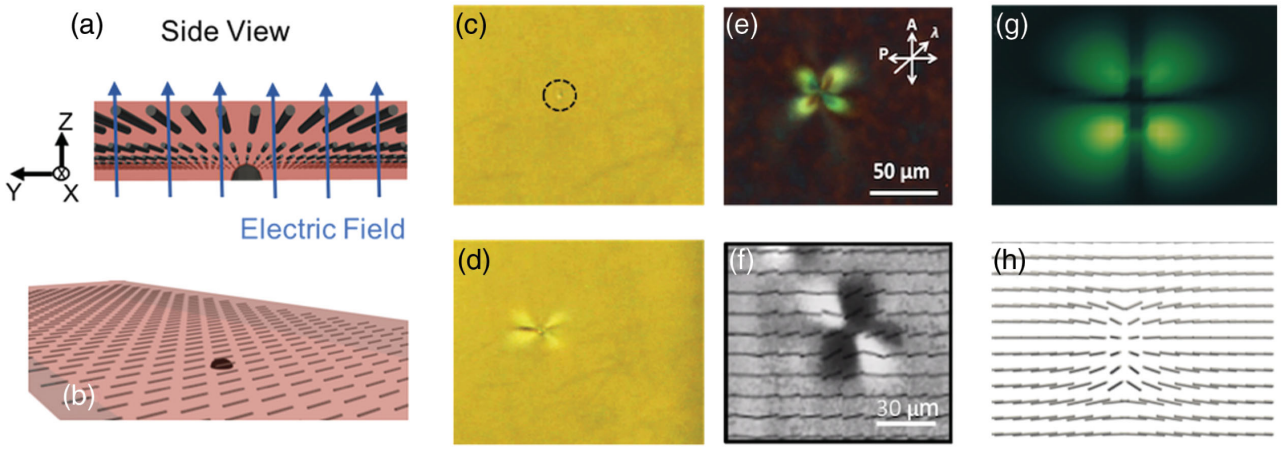

FIG. 1. Simulated system: (a) the electric field is applied perpendicular to the confining walls, which impart parallel anchoring and (b) a hemispherical particle is placed on the bottom boundary. (c) The PE particle (indicated by a black circle) in the LC film confined between two C_{16}SH SAM surfaces. (d),(e) The particle nucleates a stationary quadrupolar distortion when an electric field (300 Hz, 40 V) is applied; (d) bright-field image, (e) imaged under crossed polarizers. Scale bars 50 μm. The results of simulations of the butterfly structure are consistent with the experimental observations. Experimentally, it is observed that the butterfly remains stable in the vicinity of the particle. (f) Polscope image showing the LC director profiles within a stationary butterfly. Scale bar 30 μm. (g) In simulations, polarized light shows the butterfly in the region of the hemisphere with a 1 μm size, and (h) the orientation of the director matches the experimental observation.

The structure of the nematic director field in the midplane of the channel is shown in Fig. 1. Note that, in the absence of the applied field, the director in the midplane is undisturbed and is aligned along the X axis. For a low EF^*, when the flexoelectric energy is smaller than the elastic energy intensity ($EF^* < 1.0$), the flexoelectricity contribution is negligible and the orientation of the director remains unchanged. The cross-polarized light micrographs were calculated using a Jones matrix, with the incident polarized wave vector propagated along the Z axis.

When a slightly higher EF^* is applied ($1.0 < EF^* < 1.5$), and the flexoelectric energy becomes comparable to the elastic energy, the flexoelectricity has a strong influence around the particle surface, leading to the formation of a quadrupolar structure (a butterfly structure). The analysis of the director field profile and cross-polarized light simulations show that the director orientation is more distorted and further tilted in the third dimension for the butterfly. As shown in Fig. 1, the simulated polarized light image is consistent with our experimental observations above a small spherical particle. In all cases, if the electric field is removed, the system returns to the homogenous configuration after 2000 steps (see Fig. S2 in Supplemental Material [43]); we define that timescale as the characteristic relaxation time (τ) and the characteristic frequency* as τ/steps.

Our experiments and simulations show that for a higher applied EF^* ($EF^* = 1.7$ & $10 <$ frequency*), the energy of the system starts to increase, and the butterfly adopts an asymmetric structure that tilts towards the negative Y axis. At some point, the butterfly structure releases a propagating soliton or "bullet," which can be seen in our experiments [Fig. 2(a)] and simulations [Fig. 2(b)]. Figure 2(c) shows all contributions to the free energy of the system. When the ac field is applied, the energy of the system gradually increases and, upon the bullet's detachment, it drops and remains almost flat. It then increases again until a new bullet is released. After leaving the butterfly, the bullet moves in a direction perpendicular to the X axis [Fig. 2(b)], consistent with our experimental observations [Fig. 2(a)]. The process continues as new bullets are created and emitted from the butterfly (see movie 1 in the Supplemental Material [43]). This 3D soliton structure (see Fig. S3 in the Supplemental Material [43]) is facilitated by the thin channel because the strong anchoring energy causes the director to return to a homogenous configuration after the bullet advances along the channel; note that for the anchoring strength considered here, the surface contribution is 2 orders of magnitude smaller than the other contributions to the free energy [Fig. 2(f)], but it is sufficient to force the director field to return to the homogeneous orientation after the 3D soliton structure moves away. The other contributions to the free energy (i.e., Landau–de Gennes, elastic, flexoelectric energy) adopt higher values after each bullet is generated. After the bullet becomes detached from the butterfly, the energy drops but not all the way to the butterfly state, because the entire system now includes the butterfly and the bullet. With each new bullet, the free energy of the system increases [Fig. 2(c)]. The dielectric energy exhibits a nearly monotonic behavior (except for the random noise) throughout the entire process [Fig. 2(e)] and, for that reason, it is not included in the total free energy plot shown in Fig. 2(c).

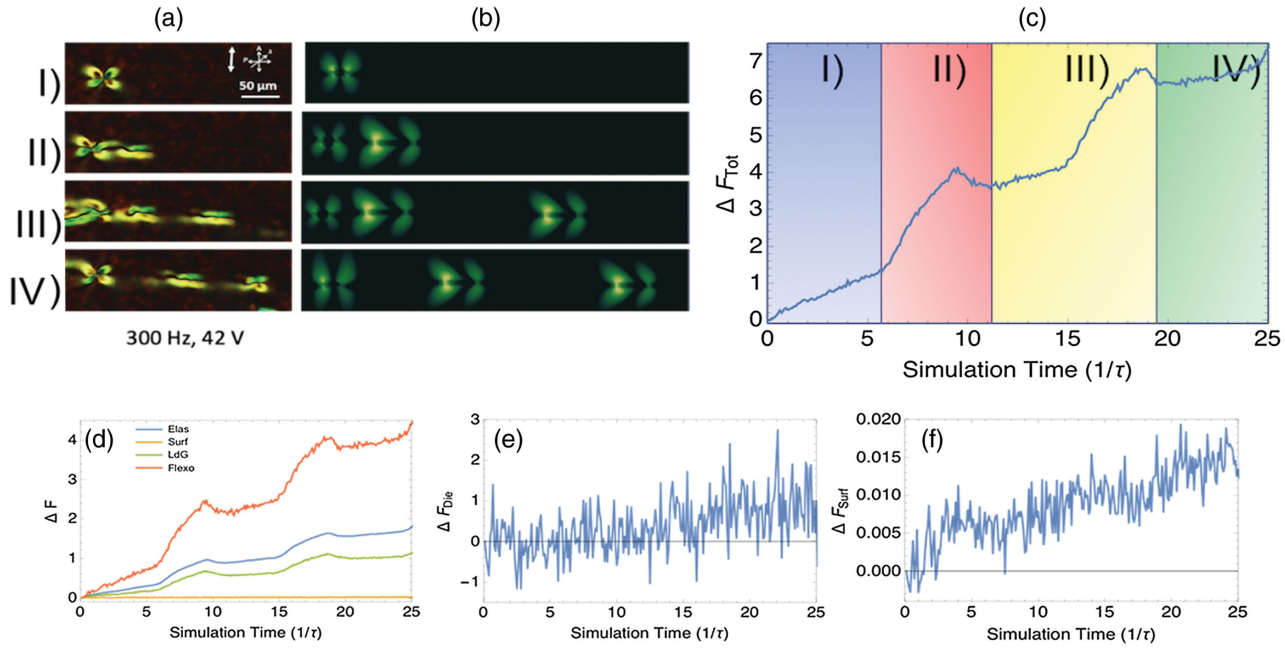

FIG. 2. (a) Experimental observation of bullet release from a butterfly. (b) Corresponding simulation results show the creation of a butterfly in the region above the particle, and the repeated ejection of bullets that move with uniform speed. (c) Free energy as a function of simulation time; the energy increases until a bullet becomes detached from the butterfly, at which point the energy drops slightly before another bullet is ejected. Each colored region corresponds to the ejection of a new bullet. (d) Landau–de Gennes, elastic and flexoelectric, and surface energy contribution, respectively. (e) The dielectric energy exhibits a small increase throughout the entire process. (f) The surface energy is 2 orders of magnitude smaller than the other contributions to the free energy; it increases with each bullet that is formed.

Figure 3 shows a state diagram, which outlines the five structures that our model predicts as a function of the frequency* and intensity of the electric field*. Starting from a low intensity ($EF^* < 1.0$), we find that the anchoring of the particle determines the orientation of the director, leading to a cross pattern under cross polarizers. Upon increasing the intensity ($1.0 < EF^* < 1.5$), we observe that a butterfly is formed, where the flexoelectric contribution begins to change the orientation of the director. Above a threshold, EF^* strength ($EF^* = 1.7$ & $10 <$ frequency*),

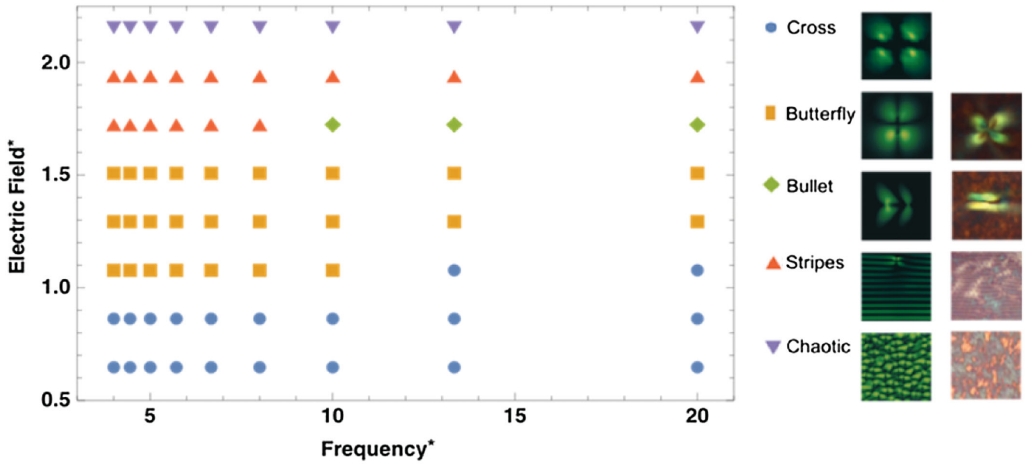

FIG. 3. State diagram delineating regions where different structures are observed as a function of the normalized frequency and intensity of the electric field. We show the director's corresponding theoretical and experimental images under cross polarizers, respectively; starting from low intensity, we observe a cross pattern above the particle. After increasing the intensity, a butterfly is observed and bullets are generated in a narrow region of frequency. Stripes are observed for a high-intensity field over a wide range of frequencies. The system enters a chaotic regime when the electric field is even stronger.

a soliton (bullet) is formed, which travels in the direction perpendicular to the initial director orientation. When the intensity of the EF^* is increased ($1.8 < EF^* < 2.0$) even more, the flexoelectric contribution distorts the entire system homogeneously, and lines (stripes) are formed in the direction parallel to the orientation of the director; the stripes move perpendicularly to the director. For an even stronger EF^* ($2.0 < EF^*$), the system enters a chaotic regime (see Fig. S5 in the Supplemental Material [43]) and the free energy is 2 orders of magnitude higher than the energy of the bullet. Our experiments confirm the general predictions of the theory.

Conclusions.—The minimal model adopted here includes contributions from surface energy, elasticity, and flexoelectricity. Our experimental system consists of a nematic liquid crystal confined between two plates, and adsorbed particles that promote soliton formation. The system is charge neutral but, while we did not add any ionic species to our experiments, we acknowledge that it is difficult to remove trace amounts of ions in LC films. However, the results of our simulations confirm that solitonic structures can be created without ionic effects. A surface inhomogeneity (a hemispherical particle) is necessary to "seed" the formation of a butterfly, which is generated upon application of an ac field. Above a threshold intensity value, the butterfly ejects solitons or bullets that travel with uniform velocity throughout the system. The butterfly and the bullets have a quadrupolar structure. At higher field strengths, our simulations reveal the formation of stripes. For even stronger fields we find evidence of a chaotic regime. The general phenomenology predicted in simulations is consistent with our own experimental observations.

Our results indicate that flexoelectricity plays a key role in the formation of solitons. At rest, the butterfly is stabilized by the balance between flexoelectricity, enthalpic energy, anchoring, and elasticity. Above a threshold field intensity, that balance is altered—the flexoelectric contribution rises and the total energy increases to a maximum when the incipient bullet touches the surface of the hemispherical particle. The bullet becomes detached from the particle at that moment, and the total energy decreases again until a new bullet is generated.

Note that, for our model, bullets are only observed over a narrow region of field intensity and frequency, and they are susceptible to the nature of the surface imperfection (size, strength anchoring, and anchoring type of the hemispherical particle). Building on the work presented here, it should be possible to further refine the model by incorporating the effects of unequal elastic constants, hydrodynamic effects, and ionic effects, which will all serve to provide a comprehensive description of soliton structure and dynamics. That work would appear to be warranted, given that a better understanding of soliton dynamics could lead to applications in microfluidic separations, reactions, or sensing, where fast transport offers distinct advantages.

This work was supported by the Department of Energy, Basic Energy Sciences, Division of Materials Research, Biomaterials Program under Grant No. DESC0019762. N. A. acknowledges support from a MRSEC-funded Kadanoff-Rice fellowship (DMR-2011854).

*These authors contributed equally to this work.
†depablo@uchicago.edu

[1] N. J. Zabusky and M. D. Kruskal, Phys. Rev. Lett. **15**, 240 (1965).
[2] N. Manton and P. Sutcliffe, *Topological Solitons*, Cambridge Monographs on Mathematical Physics (Cambridge University Press, Cambridge, England, 2004).
[3] T. Dauxois and M. Peyrard, *Physics of Solitons* (Cambridge University Press, Cambridge, England, 2006).
[4] P. G. De Gennes, J. Phys. **32**, 789 (1971).
[5] L. Leger, Solid State Commun. **11**, 1499 (1972).
[6] H. R. Brand, C. Fradin, P. Finn, W. Pesch, and P. Cladis, Phys. Lett. A **235**, 508 (1997).
[7] B.-X. Li, V. Borshch, R.-L. Xiao, S. Paladugu, T. Turiv, S. V. Shiyanovskii, and O. D. Lavrentovich, Nat. Commun. **9**, 2912 (2018).
[8] A. Earls and M. C. Calderer, Liq. Cryst. **49**, 742 (2022).
[9] Y. Shen and I. Dierking, Soft Matter **16**, 5325 (2020).
[10] B.-X. Li, R.-L. Xiao, S. Paladugu, S. V. Shiyanovskii, and O. D. Lavrentovich, Nat. Commun. **10**, 3749 (2019).
[11] S. Aya and F. Araoka, Nat. Commun. **11**, 3248 (2020).
[12] Y. Shen and I. Dierking, Commun. Phys. **3**, 14 (2020).
[13] X. Tang, A. Mozaffari, N. Atzin, S. Das, N. L. Abbott, and J. J. de Pablo, arXiv:2211.01453.
[14] R. Zhang, A. Mozaffari, and J. J. de Pablo, Nat. Rev. Mater. **6**, 437 (2021).
[15] L. Lam, Solitons and field induced solitons in liquid crystals, in *Solitons in Liquid Crystals*, edited by L. Lam and J. Prost (Springer, New York, New York, NY, 1992), pp. 9–50.
[16] W. Helfrich, J. Chem. Phys. **51**, 4092 (1969).
[17] Y. Shen and I. Dierking, Crystals **12**, 94 (2022).
[18] O. D. Lavrentovich, Liq. Cryst. Rev. **8**, 59 (2020).
[19] S. Das, S. Roh, N. Atzin, A. Mozaffari, X. Tang, J. J. de Pablo, and N. L. Abbott, Langmuir **38**, 3575 (2022).
[20] S. Das, N. Atzin, X. Tang, A. Mozaffari, J. de Pablo, and N. L. Abbott, Phys. Rev. Lett. **131**, 098101 (2023).
[21] A. Mozaffari, R. Zhang, N. Atzin, and J. J. de Pablo, Phys. Rev. Lett. **126**, 227801 (2021).
[22] J. C. Armas-Pérez, J. P. Hernández-Ortiz, and J. J. de Pablo, J. Chem. Phys. **143**, 243157 (2015).
[23] J. C. Armas-Pérez, A. Londono-Hurtado, O. Guzmán, J. P. Hernández-Ortiz, and J. J. de Pablo, J. Chem. Phys. **143**, 44107 (2015).
[24] A. N. Beris and B. J. Edwards, *Thermodynamics of Flowing Systems: With Internal Microstructure*, Oxford Engineering Science Series (Oxford University Press, New York, 1994).

[25] J. Shechter, N. Atzin, A. Mozaffari, R. Zhang, Y. Zhou, B. Strain, L. M. Oster, J. J. de Pablo, and J. L. Ross, Langmuir **36**, 7074 (2020).
[26] H. Yokoyama, Phys. Rev. E **55**, 2938 (1997).
[27] A. Londoño-Hurtado, J. C. Armas-Pérez, J. P. Hernández-Ortiz, and J. J. De Pablo, Soft Matter **11**, 5067 (2015).
[28] P. G. de Gennes and J. Prost, *The Physics of Liquid Crystals* (Oxford Science Publications, New York, 1995).
[29] P. G. De Gennes, Phys. Lett. **30A**, 454 (1969).
[30] P. M. Chaikin and T. C. Lubensky, *Principles of Condensed Matter Physics* (Cambridge University Press, Cambridge, England, 1995).
[31] H. Mori, E. C. Gartland, J. R. Kelly, and P. J. Bos, Jpn. J. Appl. Phys. Part 1 **38**, 135 (1999).
[32] J. Nehring and A. Saupe, J. Chem. Phys. **56**, 5527 (1972).
[33] L. D. Landau, E. M. Lifshitz, and L. P. Pitaevskii, *Electrodynamics of Continuous Media (Second Edition)*, 2nd ed. (Butterworth-Heinemann, London, 1984).
[34] A. L. Alexe-Ionescu, Phys. Lett. A **180**, 456 (1993).
[35] M. L. Blow and M. M. Telo Da Gama, J. Phys. Condens. Matter **25**, 245103 (2013).
[36] L. D. Landau and E. M. Lifshitz, *Fluid Mechanics: Landau and Lifshitz: Course of Theoretical Physics, Volume 6* (Elsevier Science, New York, 2013).
[37] T. Porenta, M. Ravnik, and S. Zumer, Soft Matter **7**, 132 (2011).
[38] L. A. Parry-Jones, R. B. Meyer, and S. J. Elston, J. Appl. Phys. **106**, 14510 (2009).
[39] S. P. Palto, N. J. Mottram, and M. A. Osipov, Phys. Rev. E **75**, 061707 (2007).
[40] A. Rapini and M. Papoular, J. Phys. Colloques **30**, C4 (1969).
[41] M. Papoular and A. Rapini, Solid State Commun. **7**, 1639 (1969).
[42] J.-B. Fournier and P. Galatola, Europhys. Lett. **72**, 403 (2005).
[43] See Supplemental Material at http://link.aps.org/supplemental/10.1103/PhysRevLett.131.188101 for a detailed discussion of the theoretical framework, numerical simulation, experimental information, and figures/movies of the soliton structure.
[44] T. A. Osswald and J. P. Hernández-Ortiz, Modeling and Simulation. Munich: Hanser, Polym. Process. (2006).
[45] N. Kumar, R. Zhang, J. J. de Pablo, and M. L. Gardel, Sci. Adv. **4**, eaat7779 (2018).
[46] Z. Guo and C. Shu, *Lattice Boltzmann Method And Its Application In Engineering*, Advances In Computational Fluid Dynamics (World Scientific Publishing Company, New York, 2013).
[47] N. Atzin, O. Guzmán, O. Gutiérrez, L. S. Hirst, and S. Ghosh, Phys. Rev. E **97**, 062704 (2018).